Communications in Theoretical Physics

Commun. Theor. Phys. **77** (2025) 075501 (6pp) https://doi.org/10.1088/1572-9494/adac3b
CSTR: 32041.14.CTP.adac3b

Elastic scattering of metastable positronium from antihydrogen

Yi Zhang[1,2] **and Jun-Yi Zhang**[3]

[1] Center for Theoretical Physics, Hainan University, Haikou 570228, China
[2] School of Physics and Optoelectronic Engineering, Hainan University, Haikou 570228, China
[3] State Key Laboratory of Magnetic Resonance and Atomic and Molecular Physics, Wuhan Institute of Physics and Mathematics, Chinese Academy of Sciences, Wuhan 430071, China

E-mail: yzhang@hainanu.edu.cn and jzhang@apm.ac.cn

Received 18 November 2024, revised 20 January 2025
Accepted for publication 21 January 2025
Published 7 April 2025

Abstract

The study of collision between metastable positronium (Ps) and antihydrogen ($\bar{\mathrm{H}}$) is crucial for precision experiments involving $\bar{\mathrm{H}}$. In this paper, we investigate the elastic scattering between $\bar{\mathrm{H}}$ and Ps($2s$) by combining the confined variational method with the projection method, for scattering energies from 0.0245 eV to 0.068 eV. Our calculations provide accurate phase shifts and cross sections for the $^{1,3}S$ and $^{1,3}P$ symmetries. Near the binding threshold, the rapid increase in the total cross section may be attributed to the P-wave resonance effect. Additionally, we determined the S-wave scattering lengths to be 9.34 a_0 and 5.81 a_0 for singlet and triplet elastic scattering, respectively.

Keywords: elastic scattering, positronium, antihydrogen

1. Introduction

Antihydrogen ($\bar{\mathrm{H}}$) consists of an antiproton ($\bar{p}$) and a positron (e^+), making it the antimatter counterpart to the hydrogen atom. $\bar{\mathrm{H}}$ has been an important object for precise investigations to verify fundamental principles and uncover new physics, utilizing spectral measurements to compare physical properties of H and $\bar{\mathrm{H}}$ [1, 2]. Additionally, Gravitational Behavior of Antihydrogen at Rest (GBAR) experiments with $\bar{\mathrm{H}}$ at the Extra Low Energy Antiproton ring (ELENA) facility at CERN [3] have been crucial in testing the weak equivalence principle [4–6]. In GBAR experiments, a fundamental step involves a charge-exchange reaction where excited Ps(nl) scatters by $\bar{\mathrm{H}}$, forming antihydrogen anions ($\bar{\mathrm{H}}^+$). This reaction, considered an inelastic process, has been extensively studied using various methods [7–11]. However, elastic scattering processes involving excited Ps and $\bar{\mathrm{H}}$ have received relatively less attention. As experimental techniques improve, interest in exploring lower-energy scattering processes between excited Ps and $\bar{\mathrm{H}}$ is increasing.

Due to charge-conjugation symmetry, scattering processes involving Ps and $\bar{\mathrm{H}}$ can be equivalent to Ps and H. Ground state Ps and H scattering studies are vital for understanding interactions between Ps and normal matter, leading to extensive investigations. Methods such as the static-exchange approach, diffusion Monte Carlo, close-coupling, various Kohn variational methods, stochastic variational method (SVM), and confined variational method (CVM) have been employed in these studies [12–26]. These techniques have calculated scattering phase shifts for S-, P-, and D-wave scattering, with the CVM producing exceptionally accurate low-energy phase shifts and cross-sections. Specifically, they offer highly precise phase shifts for S-, P-, and D-wave interactions at incident energies up to 3 eV [26]. The CVM could be used to exact the phase shifts from scattering wavefunction which is calculated by the projection method.

The projection method, utilizing explicitly correlated Gaussian (ECG) functions, has proven valuable in characterizing highly excited systems. This method has effectively probed resonances in doubly excited systems such as He, e^+He, Ps_2, and PsH [27–31]. By applying this method, one can obtain the wavefunction of a specific excited state of interest. Both projection methods and CVM are implemented by solving the eigenenergies of Hamiltonians that incorporate pseudopotential. Therefore, combining the projection method and CVM offers a promising approach to address low-energy scattering challenges in excited Ps.

This paper aims to combine the projection method and CVM to calculate phase shifts, scattering length and partial-wave cross-sections for $^{1,3}S$ and $^{1,3}P$ symmetries between

$\bar{\mathrm{H}}(1s)$ and Ps($2s$). The structure of this paper is as follows: sections 2.1 and 2.2 briefly introduce the projection method and CVM. The combination of the projection method and CVM are present in section 2.3. Section 3.1 presents the phase shifts and cross-sections. Section 3.2 details the calculations of the S-wave scattering length. Finally, section 4 provides a brief summary. Phase shifts are expressed in radians and atomic units (a.u.) are used throughout, unless specified otherwise.

2. Theoretical method

2.1. Projection method

The projection method has been widely used for the identification of resonance states. In this method, a penalty function is added to the Hamiltonian to enforce the exclusion of certain orbits from the active space, resulting in the autoionization of the system. This projection calculation is often called a $\hat{Q}\hat{H}\hat{Q}$ calculation. The Hamiltonian $\hat{Q}\hat{H}\hat{Q}$ is diagonalized to investigate resonant states, where $\hat{Q} = (1 - \hat{P})$ is the projection operator. In the present work, the $\hat{Q}\hat{H}\hat{Q}$ Hamiltonian is approximated by adding an OPP operator to the Hamiltonian. This method is commonly referred to as the OPP method. The energies calculated via the OPP method will converge to those calculated by diagonalizing the $\hat{Q}\hat{H}\hat{Q}$ Hamiltonian. For the calculation of $\bar{\mathrm{H}}(1s)$-Ps($2s$), the OPP operator is defined as $\sum_i \hat{P}_i = \sum_i |\phi_{Ps}(\boldsymbol{r}_i)\rangle \langle \phi_{Ps}(\boldsymbol{r}_i)|$, where $|\phi_{1S}(\boldsymbol{r}_i)\rangle$ is the wavefunction of the Ps($1s$) orbital. The choice of this penalty function effectively excludes all Ps (1s) orbitals from the system's wavefunction. After performing the variational calculation, the system's energy approaches the threshold of Ps ($2s$) + H ($1s$). The corresponding wavefunction can also be obtained. In previous work, a series of resonance states was calculated using the complex coordinate rotation method applied to this wavefunction [30].

2.2. Confined variational method

In scattering studies, directly obtaining phase shifts from a wavefunction is often difficult and imprecise. The CVM, developed earlier, addresses this by adding a confined potential into the scattering system's Hamiltonian, linking phase shifts to bound-state energy calculations [25, 26, 29, 32–34]. According to CVM theory, if two potentials V_{cp} and V_m have the same eigenenergy E_{cp} under the same confining potential V_{cp}, they will produce the same phase shift at energy E_{cp}. Suppose V_{cp} represents the actual potential between Ps($2s$) and $\bar{\mathrm{H}}(1s)$, while V_m is an auxiliary and adjustable potential. The CVM allows us to construct this auxiliary potential V_m and solve the scattering equation for V_m to determine the phase shift for the original Ps($2s$)-$\bar{\mathrm{H}}(1s)$ scattering problem.

The OPP method can approximately represent the Hamiltonian of an excited-state system. The CVM can transform the original Ps($2s$)-$\bar{\mathrm{H}}(1s)$ scattering problem into a confined Ps($2s$)-$\bar{\mathrm{H}}(1s)$ bound-state problem Therefore, we propose combining the CVM and OPP method to calculate the scattering process between Ps($2s$) and $\bar{\mathrm{H}}(1s)$.

2.3. Combination of the CVM and OPP method

The combination of these two methods can be implemented by adding both the confined potential operator and the OPP operator into the real Hamiltonian. The encompassing equation can be expressed as:

$$(H + \lambda P + V_{\mathrm{cp}})\Psi(\boldsymbol{r}, \boldsymbol{s}) = E_{\mathrm{cp}}\Psi(\boldsymbol{r}, \boldsymbol{s}), \tag{1}$$

$$H = -\frac{1}{2}\sum_{i=1}^{3}\nabla_i^2 \; - \sum_{i=1}^{3}\frac{q_i}{r_i} + \sum_{\substack{i,j=1 \\ i<j}}^{3}\frac{q_i\, q_j}{|\boldsymbol{r}_{ij}|}, \tag{2}$$

where the antihydrogen's nuclear mass is assumed to be infinite, and $\boldsymbol{r}_1$, $\boldsymbol{r}_2$ represent the positions of two positrons relative to the fixed nucleus while $\boldsymbol{r}_3$ represents an electron. Thus $\boldsymbol{r}^{\mathrm{T}}$ denotes ($\boldsymbol{r}_1$, $\boldsymbol{r}_2$, $\boldsymbol{r}_3$), $\boldsymbol{s}^{\mathrm{T}} = (\boldsymbol{s}_1, \boldsymbol{s}_2, \boldsymbol{s}_3)$ is the spins of these particles, and $\boldsymbol{r}_{ij} = |\boldsymbol{r}_i - \boldsymbol{r}_j|$. The charge of the electron and positron are denoted by q_i. The confined potential V_{cp} is:

$$V_{\mathrm{cp}} = \sum_{i=1}^{2} v_{\mathrm{cp}}(\rho_i)\,, \tag{3}$$

where

$$v_{\mathrm{cp}}(\rho_i) = \begin{cases} 0, & \rho_i < R_0\,, \\ G(\rho_i - R_0)^2, & \rho_i \geqslant R_0\,, \end{cases}$$

which is 0 for $\rho_i < R_0$ and increases quadratically beyond R_0. Here, $\rho_i = |\boldsymbol{r}_i + \boldsymbol{r}_3|/2$ is the distance between the antihydrogen nucleus and the Ps center-of-mass, and R_0 is chosen to ignore complex short-range interactions between Ps and $\bar{\mathrm{H}}$ outside the sphere of radius R_0.

To elevate the total energy E_{cp} to the excited threshold of Ps($2s$)+$\bar{\mathrm{H}}(1s)$, the OPP operator can be defined as follows:

$$P = |\phi_{Ps}(\boldsymbol{r}_{13})\rangle \langle \phi_{Ps}(\boldsymbol{r}_{13})| + |\phi_{Ps}(\boldsymbol{r}_{23})\rangle \langle \phi_{Ps}(\boldsymbol{r}_{23})|\,. \tag{4}$$

Here, the Ps($1s$) wavefunction $\phi_{\mathrm{Ps}}(\boldsymbol{r}_{ij})$ is represented using a linear combination of 10 ECGs resulting in a ground-state energy eigenvalue of -0.249999. Based on previous computational experience, the parameter λ is set to 10^4. This value, lower than previous settings, effectively reduces numerical issues while preserving an acceptable level of computational precision.

In this study, we employ an ECG basis to expand the wavefunction of the PsH system. The E_{OPP} approaches the threshold energy of Ps($2s$)+$\bar{\mathrm{H}}(1s)$, facilitating an accurate depiction of correlations among charged particles [26, 35–37]. The ECG basis functions are given by:

$$\psi_n(\boldsymbol{r}, \boldsymbol{s}) = |\boldsymbol{\nu}|^{2K+L} \exp\left(-\frac{1}{2}\boldsymbol{r}^{\mathrm{T}}A^{(n)}\boldsymbol{r}\right) Y_{LM}(\boldsymbol{\nu})\chi(\boldsymbol{s}), \tag{5}$$

where L is the system's total orbital angular momentum, and $\boldsymbol{\nu} = \boldsymbol{u}^{\mathrm{T}}\boldsymbol{r}$ with $\boldsymbol{u}^{\mathrm{T}} = (u_1, u_2, u_3)$ representing a global vector associated with L. The function $\chi(\boldsymbol{s})$ denotes the total electronic spin, set as the spin-singlet or spin-triplet state in this study. The matrix $A^{(n)}$, comprising independent parameters $A_{ij}^{(n)}$ in an $n \times n$ symmetric configuration, is optimized via

energy minimization using the stochastic variational method. To accommodate the increased nodes in excited states, the pre-exponential factor $|\boldsymbol{\nu}|^{2K+L}$ is introduced, where K is an integer.

We incorporate the OPP operator and confined potential in equation (1) to specify the total energy $E_{\rm cp}$, defined as $E_{\rm cp} = E_k + E_{\rm OPP}$. Here, $E_k = k^2/2\mu$ is the scattering energy of the Ps and $E_{\rm OPP} = E_{\bar{\rm H}(1s)} + E_{Ps(2s)} = -0.5 - 0.0625 = -0.5625$ is the threshold energy of Ps(2s)+$\bar{\rm H}$(1s). The value of $E_{\rm cp}$ can be adjusted to match a specific momentum k for scattering. μ is the reduced mass between Ps and $\bar{\rm H}$, taken as 2 in the case of infinite nuclear mass. For instance, for an excited Ps(2s) projectile with momentum $k = 0.1$, $E_{\rm cp}$ should be adjusted to -0.56 by change the parameter G in confined potential $V_{\rm cp}(\rho)$. With the confined potential $V_{\rm cp}(\rho)$ established, we solve the one-dimensional bound-state problem:

$$\left(-\frac{1}{2\mu}\frac{{\rm d}^2}{{\rm d}\rho^2} + \frac{l(l+1)}{2\mu\rho^2} + V_m(\rho) + V_{\rm cp}(\rho)\right)\Phi(\rho) = E_k\Phi(\rho), \tag{6}$$

$\Phi(\rho)$ is the eigenfunction corresponding to the eigenvalue E_k, equal to the scattering energy. Additionally, the tunable model potential $V_m(\rho)$ is defined as:

$$V_m(\rho) = \eta {\rm e}^{-\alpha\rho} - \frac{C_6}{\rho^6}(1 - {\rm e}^{-(\rho/\beta)^6}). \tag{7}$$

Here, η, α, and β are adjustable parameters, and C_6 is the van der Waals coefficient between Ps(2s) and $\bar{\rm H}$(1s), calculated as 242.4 based on our method described in previous research [29]. The term $-C_6/\rho^6$ in $V_m(\rho)$ aims to accurately describe the interaction between Ps and H in the asymptotic region, i.e., outside the sphere of radius R_0. In this study, α is fixed at 0.5 and β at 5, while η is varied to ensure the bound-state problem equation (6) produces the eigenvalue E_k for a given k. Finally, we solve the scattering equation for the potential $V_m(\rho)$ alone:

$$\left(-\frac{1}{2\mu}\frac{{\rm d}^2}{{\rm d}\rho^2} + \frac{l(l+1)}{2\mu\rho^2} + V_m(\rho)\right)\Phi'(\rho) = E_k\Phi'(\rho), \tag{8}$$

using an integration procedure to determine the scattering phase shift δ_L^k. This is achieved through a least-square fit between δ_L^k and $A\sin(k\rho - \ell\pi/2 + \delta_L^k)/(k\rho)$ for $\rho \to \infty$. It's important to note that these transformations from the original many-body scattering problem to equations (1), (6), and then (8) ensure that the logarithmic derivatives of the wave functions determined by these equations are consistent at the radial boundary R_0.

In summary, the combination of the OPP method and the CVM offers new perspectives on the Ps(2s)-$\bar{\rm H}$(1s) interactions. The Hamiltonian, as expressed in equation (1), for the Ps(2s)-$\bar{\rm H}$(1s) system, using the OPP operator and a confined potential, effectively represents the Ps(2s)-$\bar{\rm H}$(1s) scattering. After performing the variational calculation of equation (1) within the ECG basis, the confined potential corresponding to each scattering energy E_k is obtained. Subsequently, the model potential parameters can be determined using equation (6), and the scattering phase shift at this scattering energy can be calculated using equation (8).

Table 1. The convergence tests for the triplet S-wave phase shifts ${}^{-}\delta_0^{0.1}$ (in radians) at $k = 0.1$ for Ps(2s)-$\bar{\rm H}$(1s) scattering as the confined range R_0 and basis deminsions N increases. In atomic units.

N	${}^{-}\delta_0^{0.1}$	R_0	${}^{-}\delta_0^{0.1}$
1600	−0.468	27	−0.469
1800	−0.466	28	−0.466
2000	−0.465	29	−0.465
2200	−0.465	30	−0.465

Table 2. The singlet and triplet S- and P-wave phase shifts ${}^{\pm}\delta_L^k$ (in radians) for Ps(2s)-$\bar{\rm H}$(1s) scattering obtained by the CVM combined with projection method at $k = 0.06$-0.1. In atomic units.

k	${}^{-}\delta_0^k$	${}^{-}\delta_1^k$	${}^{+}\delta_0^k$	${}^{+}\delta_1^k$
0.06	−0.316	1.18	−0.476	0.975
0.07	−0.359	1.12	−0.530	0.918
0.08	−0.397	1.07	−0.575	0.857
0.09	−0.429	1.02	−0.615	0.790
0.1	−0.465	0.968	−0.656	0.732

3. Results and discussion

3.1. Phase shifts and cross sections

In this section, we combine the CVM and OPP methods based on the ECG basis to extract the Ps(2s)-$\bar{\rm H}$(1s) phase shifts. In this work, we use the symbol ${}^{\pm}\delta_L^k$ to denote phase shifts at specific incident momenta k, with the subscript $L = 0$, 1 indicating S-wave and P-wave, respectively. The superscripts '+' and ' − ' represent the singlet and triplet states, respectively. This is the first implementation of these combined methods, so we performed preliminary convergence tests for phase shifts over confined range R_0 and basis dimensions N, with results in table 1, which shows that phase shifts converge with increasing R_0 and N. Using $R_0 = 30$ and $N = 2200$, we achieve three-digit convergence for ${}^{-}\delta_0^{0.1}$ in Ps(2s)-$\bar{\rm H}$(1s) scattering. The phase shift precision for Ps(2s) is notably lower than that for Ps(1s), which achieves five-digit accuracy at the same k [26]. This discrepancy stems from the increased computational complexity introduced by the OPP operator. Consequently, we limit our computations to case with incident kinetic momentum $k \leqslant 0.1$, as higher values substantially increase computational demands. We use $R_0 = 30$ and $N = 2200$ for calculating Ps(2s)-$\bar{\rm H}$(1s) scattering.

Table 2 presents the S- and P-wave phase shifts (${}^{\pm}\delta_L^k$) for Ps(2s)-$\bar{\rm H}$(1s) scattering, derived using the CVM and OPP method combination. Following our convergence tests, we provide phase shifts for low-energy elastic scattering within the scattering energy range of $E_k = 0.0009$ to 0.025. The results exhibit a precision of three significant figures. Using

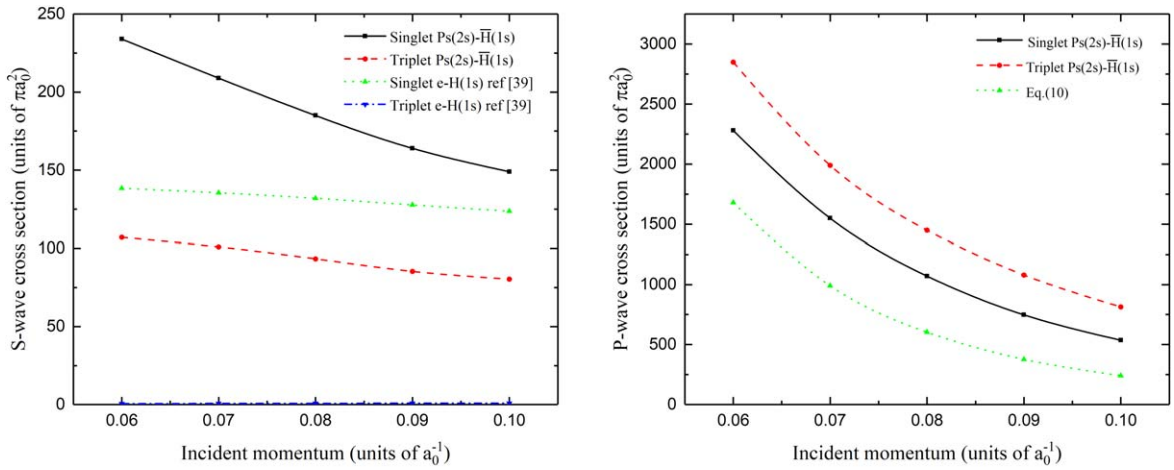

Figure 1. *S*-wave cross section for triplet and singlet Ps(2*s*)-H̄(1*s*) scattering, compared with e-H(1s) scattering (left). *P*-wave cross section for triplet and singlet Ps(2*s*)-H̄(1*s*) scattering, compared with singlet *P*-wave resonance scattering using equation (10) (right).

Table 3. The singlet and triplet *S*- and *P*-wave cross-sections $\sigma_L^{\pm}(k)$ (in πa_0^2) for Ps(2*s*)-H̄(1*s*) scattering obtained by the CVM combined with projection method at k=0.06-0.1. In atomic units.

k	$\sigma_0^-(k)$	$\sigma_1^-(k)$	$\sigma_0^+(k)$	$\sigma_1^+(k)$
0.06	107	2850	234	2280
0.07	101	1990	209	1550
0.08	93.4	1450	185	1070
0.09	85.4	1080	164	748
0.1	80.4	814	149	536

the *S*- and *P*-wave phase shifts, we can calculate the corresponding partial wave cross-sections. The formula for these cross-sections, $\sigma_L^{\pm}(k)$, is defined as follows:

$$\sigma_L^{\pm}(k) = \frac{4\pi}{k^2}(2L+1)\sin^2(^{\pm}\delta_L^k). \tag{9}$$

The S- and P-wave cross-sections are listed in table 3, and the *S*- and *P*-wave scattering cross-sections are also provided in figure 1. Due to the similarity between Ps and electron exist in scattering process [38], we have also provided the low-energy cross-sections for electron and H(1*s*) scattering in figure 1 for comparison [39]. It can be observed that the *S*-wave cross-sections for singlet state electron and positronium are comparable in magnitude. Comparison shows that in low-energy elastic scattering of Ps(2*s*)-H̄(1*s*), with scattering energies from $E_k = 0.0009$ to 0.025, the *P*-wave cross-section significantly exceeds the *S*-wave cross-section. This anomaly could be interpreted as a result of resonance state scattering.

In the singlet state Ps(2*s*)-H̄(1*s*) low-energy elastic scattering, previous studies have identified a *P*-wave resonance near $E_R = -0.56398$ [30, 40]. The current calculations, covering a total energy range from $E = -0.56$ to -0.5616, show that this resonance state significantly influences the *P*-wave scattering. This effect leads to a marked increase in the *P*-wave partial scattering cross-section, particularly at lower incident kinetic energies. As for a pure resonance with zero background scattering phase shift cross section has the Lorentz shape

$$\sigma_l(E) = \frac{4\pi(2l+1)}{k^2}\left(\frac{\Gamma^2/4}{(E_R-E)^2+\Gamma^2/4}\right). \tag{10}$$

We also present the P-wave pure resonant scattering cross-section in figure 1. It can be observed that the trend of the scattering cross-section is consistent with our calculations as k approaches zero. Scattering calculations for the triplet state Ps(2*s*)-H̄(1*s*) reveal a similar phenomenon. Previous studies have not reported any resonances in the triplet state of positronium hydride. Although using the CCR method combined with OPP basis [29–31], we also have not identified any *P*-wave triplet state resonance. Despite this, the increase in the triplet state scattering cross-section cannot be overlooked. This suggests that there may be other resonance effects or interactions in the triplet state that are not adequately captured by the current computational methods. Further research is necessary to explore the potential influences of resonance states on the triplet state scattering. This would provide a more comprehensive understanding of the underlying dynamics in these complex systems.

3.2. S-wave scattering lengths

The scattering phase shifts calculated by combining the CVM with the OPP method, which have a lower incident momentum, can be fitted under the effective range theory to obtain the *S*-wave scattering length. The effective range theory can be defined as:

$$k\cot^{\pm}\delta_0^k = -\frac{1}{a^{\pm}} + \frac{1}{2}r_0^{\pm}k^2, \tag{11}$$

where a^+ and a^- are, respectively, the singlet and triplet S-wave scattering lengths, and $r_0^{\pm}$ are the corresponding effective ranges. Considering the van der Waals interaction, equation (11) can be modified as the formula of Flannery *et al*

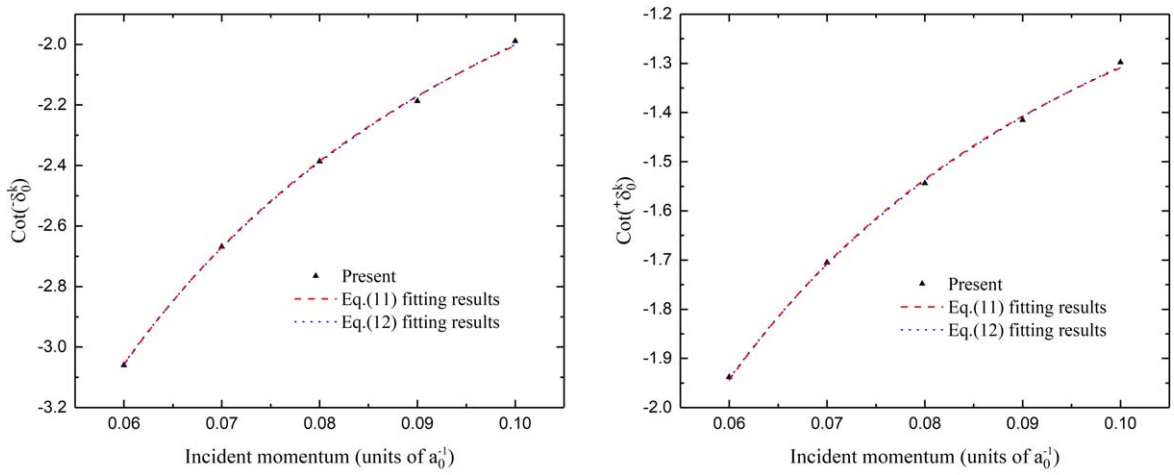

Figure 2. Scattering length fitting for triplet (left) and singlet (right) Ps(2*s*)-$\bar{\text{H}}$(1*s*) scattering.

Table 4. Comparison of singlet and triplet scattering lengths for Ps(2*s*)-$\bar{\text{H}}$(1*s*) scattering, including Ps(1*s*)-$\bar{\text{H}}$(1*s*) for reference. In atomic units.

System	Fitting formula	a^+	r_0^+	a^-	r_0^-
Ps(2*s*)-$\bar{\text{H}}$(1*s*)	Equation (11)	9.21	−4.48	5.73	−5.16
	Equation (12)	9.34	−5.53	5.81	−6.45
Ps(1*s*)-$\bar{\text{H}}$(1*s*)[a]	Equation (11)	4.2841	3.1032	2.1133	3.9563
	Equation (12)	4.2854	3.0645	2.1126	4.4759

[a] [26]

[41].

$$k\cot^{\pm}\delta_0^k = -\frac{1}{a^{\pm}} + \frac{r_0^{\pm}k^2}{2} - \frac{4\pi C_6 k^3}{15(a^{\pm})^2} - \frac{16C_6}{15a^{\pm}}k^4\ln k. \tag{12}$$

These effective range formulas are more suitable for low-k scattering situations, where higher order terms in the expansions become negligible.

Using the scattering phase shifts in table 2, we can fit the corresponding scattering length and effective range in the interval k=0.06 -0.1, which are given in table 4. The fitting curve, as shown in figure 2, can be seen that the results obtained from the two fitting methods are very similar. However, considering the large C_6 coefficient in the Ps(2*s*)-$\bar{\text{H}}$(1*s*) system, we still recommend the fitting results that take the van der Waals interaction into account. Therefore, our recommended scattering lengths are $a^+ = 9.34$ and $a^- = 5.81$, and the recommended effective ranges are $r_0^+ = -5.53$ and $r_0^- = -6.45$.

Given the lack of data on the scattering lengths of the excited state Ps(2*s*) and $\bar{\text{H}}$(1*s*), we have included the scattering lengths of the ground state Ps(1*s*) and $\bar{\text{H}}$(1*s*) in table 4 for comparison. We can find that the scattering lengths for both the ground and excited singlet states of Ps-$\bar{\text{H}}$ are approximately twice those of the corresponding triplet states. Additionally, the excited state Ps(2*s*) exhibits a longer scattering length, indicating a more extensive range of interaction with $\bar{\text{H}}$(1*s*).

It is worth noting that the current consideration of the scattering process includes only the elastic scattering channel. In real scattering process, multiple inelastic channels are present, which also contribute to the scattering length. These contributions require further detailed investigation in future studies.

4. Conclusion

This paper explores a variational method for calculating low-energy elastic scattering in excited state systems. Employing the OPP method, we accurately derived the wavefunction for the resonance state Ps(2*s*)-$\bar{\text{H}}$(1*s*), which was subsequently extended to a scattering wavefunction using the CVM. This approach enabled us to calculate low-energy *S*-wave and *P*-wave scattering phase shifts and cross-sections for Ps(2*s*)-$\bar{\text{H}}$(1*s*) elastic scattering. Notably, the cross-sections at low energies for Ps(2*s*)-$\bar{\text{H}}$(1*s*) show sharp increases, potentially indicating the influence of *P*-wave resonances. These findings affirm that the combined use of the OPP and CVM methods effectively calculates scattering parameters in excited states and may be applicable to other excited state systems as well. The calculated low-energy scattering parameters could serve as crucial references for the forthcoming Ps(2*s*)-$\bar{\text{H}}$(1*s*) scattering experiments.

Acknowledgments

This work was supported by the National Natural Science Foundation of China under Grant Nos. 12174399, 12147146 and 11934014, by the Natural Science Foundation of Hainan Province under Grant No. 122QN219, through the Innovational Fund for Scientific and Technological Personnel of

Hainan Province and by the Natural Science Foundation of Shandong Provincial under Grant No. ZR2021QA046.

ORCID iDs

Jun-Yi Zhang https://orcid.org/0000-0001-6355-2732

References

[1] Ahmadi M *et al* 2018 Characterization of the 1S–2S transition in antihydrogen *Nature* **557** 71

[2] Ahmadi M *et al* 2018 Observation of the 1S–2P Lyman-α transition in antihydrogen *Nature* **561** 211

[3] Bartmann W, Belochitskii P, Breuker H, Butin F, Carli C, Eriksson T, Oelert W, Ostojic R, Pasinelli S and Tranquille G 2018 The ELENA facility *Philos. Trans. Royal Soc.* A **376** 20170266

[4] Indelicato P *et al* 2014 The Gbar project, or how does antimatter fall? *Hyperfine Interact.* **228** 141

[5] Perez P and Sacquin Y 2012 The GBAR experiment: gravitational behaviour of antihydrogen at rest *Class. Quantum Grav.* **29** 184008

[6] Pérez P *et al* 2015 The GBAR antimatter gravity experiment *Hyperfine Interact.* **233** 21

[7] Comini P and Hervieux P-A 2013 H^+ ion production from collisions between antiprotons and excited positronium: cross sections calculations in the framework of the GBAR experiment *New J. Phys.* **15** 095022

[8] Comini P, Hervieux P-A and Biraben F 2014 H^+ production from collisions between positronium and keV antiprotons for GBAR *Hyperfine Interact.* **228** 159

[9] Comini P, Hervieux P-A and Lévêque-Simon K 2021 Corrigendum: H^+ ion production from collisions between antiprotons and excited positronium: cross sections calculations in the framework of the GBAR experiment *New J. Phys.* **23** 029501

[10] Yamashita T, Kino Y, Hiyama E, Jonsell S and Froelich P 2022 Near-threshold behavior of positronium-antihydrogen scattering cross sections *Phys. Rev.* A **105** 052812

[11] Yamashita T, Hiyama E, Piszczatowski K, Jonsell S and Froelich P 2023 A four-body calculation of s-wave resonant scattering between positronium and antihydrogen atom *4th Japan-China Joint Workshop on Positron Science (JWPS2019)* 9 *(Nara, Japan, October 28, 2019 - November 02, 2019)* (JJAP Conference Proceedings) 011002

[12] Ray H and Ghosh A S 1997 Positronium - hydrogen-atom scattering using the static exchange model *J. Phys. B: At. Mol. Opt. Phys.* **30** 3745

[13] Ray H and Ghosh A S 1996 Positronium - hydrogen atom scattering using the static exchange model *J. Phys. B: At., Mol. Opt. Phys.* **29** 5505

[14] Chiesa S, Mella M and Morosi G 2002 Orthopositronium scattering off H and He *Phys. Rev.* A **66** 042502

[15] Walters H, Yu A, Sahoo S and Gilmore S 2004 Positronium–atom collisions *Nucl. Instrum. Methods Phys. Res. Sect.* B **221** 149

[16] Sinha P K, Chaudhury P and Ghosh A S 1997 Positronium scattering by a hydrogen molecule including exchange *J. Phys. B: At., Mol. Opt. Phys.* **30** 4643

[17] Campbell C P, McAlinden M T, MacDonald F G R S and Walters H R J 1998 Scattering of positronium by atomic hydrogen *Phys. Rev. Lett.* **80** 5097

[18] Adhikari S K and Biswas P K 1999 Positronium–hydrogen-atom scattering in a five-state model *Phys. Rev.* A **59** 2058

[19] Blackwood J E, McAlinden M T and Walters H R J 2002 Importance of the H^- channel in Ps-H scattering *Phys. Rev.* A **65** 030502

[20] Reeth P V and Humberston J W 2003 Variational calculations of s-wave positronium–hydrogen scattering *J. Phys. B: At., Mol. Opt. Phys.* **36** 1923

[21] Van Reeth P and Humberston J 2004 Low energy positronium–hydrogen scattering *Nucl. Instrum. Meth. Phys. Res. Sect.* B **221** 140

[22] Page B A P 1976 Positronium-hydrogen scattering lengths *J. Phys. B: At. Mol. Phys.* **9** 1111

[23] Woods D, Ward S J and Van Reeth P 2015 Detailed investigation of low-energy positronium-hydrogen scattering *Phys. Rev.* A **92** 022713

[24] Ivanov I A, Mitroy J and Varga K 2001 Elastic positronium-atom scattering using the stochastic variational method *Phys. Rev. Lett.* **87** 063201

[25] Zhang J-Y, Yan Z-C and Schwingenschlgl U 2012 Elastic scattering of positronium: application of the confined variational method *Europhys. Lett.* **99** 43001

[26] Wu M-S, Zhang J-Y, Qian Y, Varga K, Schwingenschlögl U and Yan Z-C 2021 Confined variational calculation of positronium-hydrogen scattering below the positronium excitation threshold *Phys. Rev.* A **103** 022817

[27] Bromley M W J, Mitroy J and Varga K 2012 Positron attachment to the He doubly excited states *Phys. Rev. Lett.* **109** 063201

[28] Mitroy J and Grineviciute J 2013 Positron attachment to the He($ns^2\ ^1Se$) states *Phys. Rev.* A **88** 022710

[29] Zhang Y, Wu M-S, Qian Y, Varga K and Zhang J-Y 2021 Calculation of spin-polarized positronium-helium ($2\ ^3S$) and electron-helium ($2\ ^3S$) scattering *Phys. Rev.* A **103** 052803

[30] Zhang Y, Wu M-S, Yan G-A, Varga K, Yan Z-C and Zhang J-Y 2023 Doubly excited autodissociating resonant states of positronium hydride *Phys. Rev.* A **108** 052813

[31] Zhang Y and Yan G-A 2024 *P*-Wave doubly excited states of positronium hydride *Int. J. Theor. Phys.* **63** 80

[32] Mitroy J, Zhang J Y and Varga K 2008 Elastic scattering using an artificial confining potential *Phys. Rev. Lett.* **101** 123201

[33] Wan J-Y, Wu M-S, Zhang J-Y and Yan Z-C 2021 Confined variational calculations of low-energy electron-helium scattering *Phys. Rev.* A **103** 042814

[34] Du W, Wu M-S, Zhang J-Y, Qian Y, Varga K and Yan Z-C 2022 Non-Born-Oppenheimer confined variational calculation of low-energy Ps-H_2 scattering *Phys. Rev.* A **105** 052809

[35] Suzuki Y, Suzuki M and Varga K 1998 Stochastic Variational Approach to Quantum-Mechanical Few-Body Problems Vol. 54 (Springer)

[36] Mitroy J, Bubin S, Horiuchi W, Suzuki Y, Adamowicz L, Cencek W, Szalewicz K, Komasa J, Blume D and Varga K 2013 Theory and application of explicitly correlated Gaussians *Rev. Mod. Phys.* **85** 693

[37] Bubin S, Pavanello M, Tung W-C, Sharkey K L and Adamowicz L 2013 Born–Oppenheimer and non-Born–Oppenheimer, atomic and molecular calculations with explicitly correlated Gaussians *Chem. Rev.* **113** 36

[38] Brawley S J, Armitage S, Beale J, Leslie D E, Williams A I and Laricchia G 2010 Electron-like scattering of positronium *Science* **330** 789

[39] Reeth P V, Woods D, Ward S J and Humberston J W 2016 Comparison of positronium, positron and electron collisions with hydrogen at low velocities *J. Phys. B: At. Mol. Opt. Phys.* **49** 114001

[40] Yan Z-C and Ho Y K 1998 *P*-wave autodissociating resonant states of positronium hydride *Phys. Rev.* A **57** R2270

[41] Drake G W 2023 *Springer Handbook of Atomic, Molecular, and Optical Physics* (Springer)